



CHORUS

This is the accepted manuscript made available via CHORUS. The article has been published as:

Potential flow in the presence of a sudden expansion: Application to capillary driven transport in porous media

Eric M. Benner and Dimiter N. Petsev

Phys. Rev. E **87**, 033008 — Published 13 March 2013

DOI: [10.1103/PhysRevE.87.033008](https://doi.org/10.1103/PhysRevE.87.033008)

Potential flow in the presence of a sudden expansion. Application to capillary driven transport in porous media

Eric M. Benner and Dimiter N. Petsev

Department of Chemical and Nuclear Engineering, University of New Mexico, Albuquerque, NM 87131, USA

We present a theoretical analysis of the capillary driven transport of liquid in porous media that undergoes a sudden expansion. The use of appropriate coordinates allows for exactly and analytically solving different cases in two and three dimensions. The time dependence of liquid front motion in an expanding porous media is shown to be different from the one dimensional Lucas-Washburn (Kolloid Z., 1918. **23**: p. 15; Phys. Rev., 1921. **17**: p. 273) results as well as from the solution for two and three-dimensional circular expansions obtained by J. Hyväluoma et al. (Phys. Rev. E, 2006. **73**: p. 036705) and Xiao et al. (Langmuir, 2012. **28**: p. 4208). These cases appear as asymptotic limits of our solutions. We also observe that capillary flow in expanding three dimensional porous materials exhibits a steady state solution for the bulk flow rate at the entrance of the expansion.

I. INTRODUCTION

Capillary driven liquid flows in porous media are ubiquitous phenomena that occur both in nature and in various practical applications.¹⁻⁸ The dynamics of such flows was first analyzed about a century ago⁹⁻¹¹ for the simple case of one dimensional transport in porous materials (capillaries) of uniform cross-section. The advancement of the liquid is driven by the capillary pressure due to the curvature of the liquid-gas interface in each individual pore. Hence the liquid should wet the pore walls with a contact angle that is less than 90° . As the liquid penetrates further into the porous material of constant cross section, the total hydrodynamic resistance increases and the bulk flow rate decreases proportionally to $t^{-1/2}$ (where t is time). This result is often referred to as the Lucas-Washburn (LW) relationship.¹⁰⁻¹¹ Strictly the LW model was derived for the flow in a single straight capillary. For a porous media the LW relationship has an average macroscopic meaning, similar to the D'Arcy equation^{6,12} with pressure drop determined by capillarity and a permeability coefficient that is a complex function of the porosity. The LW model is based on the assumption that the flow is governed by the liquid motion, and the displacement of the gas phase at the front does not practically contribute due to its much lower dynamic viscosity. The model assumes a single-phase system with a moving front, and is valid in the limit of small gas pressure and density. This has been both experimentally and theoretically shown to be reasonable for a great number of systems involving liquids moving in porous media^{4,6,13-18} including by carefully obtaining the density profile at the front.¹⁹ In the case of two immiscible liquids displacing each, the flow needs to be treated as a two-phase and will depend on both viscosities.⁶ The focus of the present paper is on liquid phase capillary flow in porous materials without entrapment of air anywhere in the wetted region.

The time behavior of liquid penetration in porous media is very different if the flow occurs in porous media that expands (or contracts) in direction of the flow. Estimations of the bulk flows in 2D and 3D expanding porous media were offered¹³⁻¹⁵ suggesting that the time dependence of the flow deviates from the LW one-dimensional (1D) case. The cases of 2D radial flow where the front is represented by a gradually expanding circle was analyzed in detail by Hyväluoma et al.¹⁷ The authors compared the capillary driven flow D'Arcy type model to Lattice-Boltzmann simulation and obtained excellent agreement, thus validating the analytical approach. The detailed analysis of the 3D case corresponding to an expanding spherical surface was performed by Xiao et al.¹⁶ There the capillary driven transport model was tested against carefully performed experiments and again both were found to be in agreement. To maintain circular or spherical symmetries the flows must start from a point or an already circular (for 2D) or spherical (3D) boundary. Hyväluoma et al.¹⁷ used the model to describe the penetration of liquid in two dimensions (2D) from a droplet with circular circumference sitting on porous paper. They showed that the liquid velocity decreases with time following a different and more complicated dependence. Xiao et al.¹⁶ used the spherical expansion model to fit experimental data on capillary penetration of water in packed glass beads. All these results are very important because they imply that the shape of the porous material leads to qualitative differences in the resulting flow patterns. This means that applications using capillary driven transport in porous media can be optimized by simply shaping the materials accordingly.⁴

In this paper we present exact analytical results for the flow in porous media that exhibit sudden expansion (see Figure 1). The flow in these cases is not necessarily radial as in the Refs.¹⁶⁻¹⁷ because the entrance to the expanding porous space has finite dimension and is usually flat instead of circular. Our results include a linear velocity field at each point (on a scale greater than the typical average pore size) in the domain of interest. The detailed knowledge of the local fluid velocity is very important for applications like designing paper based diagnostic devices with different shapes,^{2,4} delivering solutions to power fuel cells⁸ or to better understanding how moisture penetrates construction materials.¹³⁻¹⁴ We derive the position of the wetted front as well as the bulk flow rate in the porous material as functions of the elapsed time. The 2D solution is applicable to a wide variety of shapes. The 3D case can be simply treated only if the domain has axial symmetry. We will limit our analysis only to porous domains with zero flow across the side boundaries and will ignore inertia effects. Inertia and hydrodynamic nonlinearity is important in the initial moment of liquid penetration into the porous media and depends on the driving capillary pressure.²⁰ The latter is a function of the pore (capillary) radius and the wetting contact angle. As the pores may vary in size, the capillary pressure used in our model is an average over the pore size distribution, which has to be sufficiently narrow to prevent capillary fingering from occurring. It was shown that for radii of the order of 50 μm inertia is usually important. If the wetting contact angle is 0° then inertial terms might be significant down to 10 μm pore radii.²⁰ Below these pore sizes viscosity is dominant and inertia does not play a role. The solution is restricted to the assumption that gravitational effects are negligible. For approximately 2D systems this is usually reasonable even for large systems as the dimensions are commonly

orthogonal to the gravitational field. However in 3D this means that the solution degrades as the capillary pressure times the surface area approaches the weight of the fluid because this greatly distorts the front of the advancing fluid by gravitational percolation.¹⁵ Finally our analysis does not include possible evaporation of 2D surfaces or of the side boundaries for both 2D and 3D systems. The analysis of cases with permeable side boundaries and surface evaporation will be published elsewhere.²¹

In the next section, we present a general overview of the capillary driven flow in porous materials. Section III presents the derivation of results for the flow velocity in 2D expanding porous media, Section IV presents the solution for the capillary driven flow in an expanding 3D porous material, Section V discusses and compares the results for each of the respective geometries, and Section VI summarizes the conclusions.

II. GOVERNING EQUATIONS FOR THE FLOW IN POROUS MEDIA

The flow of incompressible liquid in porous media is given by the mass balance

$$\nabla \cdot \mathbf{v} = 0 \quad (1)$$

where \mathbf{v} is the linear liquid velocity on a scale that is larger than the individual pore size. For mass flux a sink or source term, Q , (e.g. evaporation, condensation, etc.) may be added to the right hand side of (1); this term is presently ignored. The liquid flow in porous media is irrotational;²² therefore the velocity can be expressed by means of the velocity potential, ϕ ,

$$\mathbf{v} = \nabla \phi = -\frac{k}{\mu} \nabla P, \quad \phi = -\frac{k}{\mu} P. \quad (2)$$

The right hand side of Eq. (2) is the D'Arcy law^{12,22} with k being the permeability of the medium, μ is the dynamic shear viscosity of the liquid, and P is the pressure that drives the flow. In the case of capillary driven flow the pressure is equal to²³

$$P_c = \gamma \cos \alpha \left(\frac{1}{R_1} + \frac{1}{R_2} \right) \quad (3)$$

where γ is the interfacial tension at the gas-liquid interface, α is the contact angle that characterizes the wetting of the solid. R_1 and R_2 are the two principal radii of curvature of the pore. Equations (1) and (2) can be combined to give

$$\nabla^2 \phi = 0. \quad (4)$$

Eq. (4) will be used to obtain expressions for the liquid flow in all cases analyzed below.

III. CAPILLARY DRIVEN FLOW IN TWO DIMENSIONAL EXPANDING POROUS MEDIA

A. Exact solution in 2D

Different examples illustrating capillary liquid transport in expanding 2D porous media are sketched in Figure 1. Figures 1a and 1b show symmetric regions with different extent of expansion. Figures 1c and 1d represent two asymmetric cases. The liquid enters the expanding region through an entrance with finite width. Because of the finite size of the entrance, the shape of the expanding liquid front is elliptical rather than circular as in the case discussed by Hyväluoma et al.¹⁷ The entrance is saturated with liquid and the pressure there equals the ambient. The front of the moving wetted region is where the liquid meets the gas phase in the pores and the pressure there is equal to the ambient minus the capillary pressure [see Eq. (3)]. Hence, we look for a solution in the domain that starts at entrance and propagates a wetted front. The problem is best defined in elliptic coordinates²⁴ (see Figure 2)

$$\begin{aligned}x &= a \cosh \eta \cos \psi \\y &= a \sinh \eta \sin \psi.\end{aligned}\tag{5}$$

The general form of Eq. (4) then becomes

$$\nabla^2 \phi = \frac{1}{a^2 (\cosh^2 \eta - \cos^2 \psi)} \left(\frac{\partial^2 \phi}{\partial \eta^2} + \frac{\partial^2 \phi}{\partial \psi^2} \right) = 0.\tag{6}$$

If there is no liquid flow across the edges of the domain that are defined by $\psi = \psi_1$ and $\psi = \psi_2$ (see Figure 1), there will be no variation of ϕ with respect to the angular variable ψ . Hence the term $\partial^2 \phi / \partial \psi^2$ can be dropped from Eq. (6) and the equation simplifies to

$$\frac{d^2 \phi}{d\eta^2} = 0.\tag{7}$$

The solution of this equation describes concentric elliptic lines that correspond to the flow potential ϕ at a given η . The boundary conditions are

$$\begin{aligned}\phi &= \phi_0 = -\frac{k}{\mu} P_c \text{ at } \eta = 0 \\ \phi &= 0 \text{ at } \eta = \eta_f\end{aligned}\tag{8}$$

where $\eta = 0$ at the entrance and $\eta = \eta_f$ at the front. The solution of Eq. (7) is then

$$\varphi = -\frac{k}{\mu} P_C \left[1 - \frac{\eta}{\eta_f} \right]. \quad (9)$$

Hence the velocity of the moving liquid is

$$v_\eta = (\nabla\varphi)_\eta = \frac{1}{a(\cosh^2 \eta - \cos^2 \psi)^{1/2}} \frac{\partial\varphi}{\partial\eta} = \frac{1}{a(\cosh^2 \eta - \cos^2 \psi)^{1/2}} \left(\frac{kP_C}{\mu} \frac{1}{\eta_f} \right). \quad (10)$$

Following the approach outlined by Washburn,¹¹ we derive an equation for the velocity of the moving front

$$\begin{aligned} v_{\eta_f} &= a(\cosh^2 \eta_f - \cos^2 \psi)^{1/2} \frac{d\eta_f}{dt} = \frac{1}{a(\cosh^2 \eta_f - \cos^2 \psi)^{1/2}} \left(\frac{\partial\varphi}{\partial\eta} \right)_{\eta=\eta_f} \\ &= \left(\frac{kP_C}{a\mu} \right) \frac{1}{(\cosh^2 \eta_f - \cos^2 \psi)^{1/2}} \frac{1}{\eta_f}. \end{aligned} \quad (11)$$

It is convenient to use a dimensionless velocity that has the form $\tilde{v}_{\eta_f} = (\mu a / kP_C) v_{\eta_f}$.

The time dependence of the position of the liquid front $\eta_f(t)$ can be derived by integrating Eq. (11)

$$\frac{kP_C}{\mu} \int_0^{\eta_f(t)} \frac{(\cosh^2 \eta'_f - \cos^2 \psi)}{(\partial\varphi / \partial\eta)_{\eta=\eta'_f}} d\eta'_f = \tilde{t}, \quad \tilde{t} = \frac{kP_C}{\mu a^2} t. \quad (12)$$

After integration and brief rearrangement Eq. (12) leads to the following relationship for the time dependent position of the liquid front

$$\eta_f \sinh(2\eta_f) - \frac{1}{2} \cosh(2\eta_f) - \cos(2\psi) \eta_f^2 + \frac{1}{2} = 4\tilde{t}. \quad (13)$$

Eq. (13) represents the dependence of the front position on time $\eta_f(\tilde{t})$. Differentiating with respect to time and multiplying it by the factor $a(\cosh^2 \eta_f - \cos^2 \psi)^{1/2}$ gives the time-dependent

velocity of the front [see the left hand side of Eq. (11)]. Alternatively $\eta_f(\tilde{t})$ can be introduced in the last line of Eq. (11) to obtain the time dependence of the linear velocity $\tilde{v}_f(\tilde{t})$.

Another quantity of interest is the volumetric flux of liquid U . It is equal to the integral over the liquid linear flow velocity across the area of the front, or [see Eq. (11)]

$$U(\tilde{t}) = \int_A \mathbf{v} \cdot \mathbf{n} dA = a \int_{\psi_1}^{\psi_2} v_{\eta_f}(\tilde{t}) [\cosh^2 \eta_f(\tilde{t}) - \cos^2 \psi]^{1/2} d\psi = \left[\frac{kP_c}{\mu \eta_f(\tilde{t})} \right] (\psi_2 - \psi_1). \quad (14)$$

Since the liquid motion occurs in 2D plane, the above result is per unit length in direction normal to the plane surface. The local linear velocity \tilde{v} will decrease with the increase of η in an expanding domain and is lowest at the front where $\eta = \eta_f$. The volumetric flux U conserves because as the linear velocity decreases the front area increases to exactly compensate for that. Both, however, will change with time. For fully open entrance ($\psi_1 = 0, \psi_2 = \pi$) one obtains

$$U(\tilde{t}) = \frac{\pi k P_c}{\mu \eta_f(\tilde{t})} \quad (15)$$

B. Asymptotic results for small and large η_f

For short times, η_f is small and we can further simplify the solution (13) (also setting $\psi = \pi/2$) to read

$$\frac{\eta_f^2}{2} = \tilde{t}. \quad (16)$$

This expression is formally identical to the LW result¹⁰⁻¹¹

$$\frac{L(t)^2}{2a^2} = \tilde{t} \quad (17)$$

Which describes the position of the front $L(t)$ in porous domain with constant cross-section. Hence for short times and small η_f the effect of the expansion is negligible. It is also important to stress that the short times discussed here are reflecting only the effect of the porous media geometry and are still long in comparison to the time-scale of any inertial fluid motion. Inertia (if present) occurs on a time scale that is much faster (about at fraction of a second) and practically

absent for pores with radii below 10 μm , or for even larger pores if the wetting contact angle is less than 0° .²⁰

The asymptotic result for large η_f is obtained by realizing that $\sinh(2\eta_f) \rightarrow \exp(2\eta_f)/2$ and $\cosh(2\eta_f) \rightarrow \exp(2\eta_f)/2$. At long times the asymptotic result for (13) is

$$\frac{1}{8}\eta_f \exp(2\eta_f) - \frac{1}{16}\exp(2\eta_f) = \tilde{t}. \quad (18)$$

As will be shown below, Eq. (18) is identical to the long time asymptotic results of Hyväluoma et al.,¹⁷

$$\left(\frac{R_f}{R_0}\right)^2 \ln\left(\frac{R_f}{R_0}\right)^2 - \left(\frac{R_f}{R_0}\right)^2 + 1 \approx \left(\frac{R_f}{R_0}\right)^2 \ln\left(\frac{R_f}{R_0}\right)^2 - \left(\frac{R_f}{R_0}\right)^2 = \frac{4kP_C}{\mu R_0^2} t. \quad (19)$$

R_f is the position of the expanding liquid front and R_0 is the radius of the entrance, which in their analysis must be circular. Using the relationship between polar and elliptical coordinates defined by

$$r^2 = x^2 + y^2 = a^2 (\cosh^2 \eta \cos^2 \psi + \sinh^2 \eta \sin^2 \psi) \quad (20)$$

one can write Eq. (19) in terms of η_f . Thus tracing the position of the liquid front along the y -axis we obtain

$$\frac{R_f^2}{R_0^2} = \frac{a^2}{R_0^2} \sinh^2 \eta_f + 1. \quad (21)$$

The term 1 on the right hand side of the above equation is added to ensure that $R_f/R_0 \geq 1$. Inserting (21) into (19) describes the position of the liquid front (along the y -axis) as a function of time

$$\left(\sinh^2 \eta_f + \frac{R_0^2}{a^2}\right) \ln\left(\sinh^2 \eta_f + \frac{R_0^2}{a^2}\right) - \sinh^2 \eta_f = \frac{4kP_C}{\mu a^2} t = 4\tilde{t} \quad (22)$$

The factor R_f^2/a^2 can be found from the condition that entrances for both circular and elliptical cases are the same. For $0 \leq \psi \leq \pi$ this condition reads

$$2a = \pi R_0 \text{ or } \frac{a}{R_0} = \frac{\pi}{2}. \quad (23)$$

For large η_f we have

$$\cosh^2 \eta_f \rightarrow \frac{\exp(2\eta_f)}{4}, \quad \sinh^2 \eta_f \rightarrow \frac{\exp(2\eta_f)}{4} \quad (24)$$

and

$$\frac{R_f^2}{R_0^2} = \frac{a^2}{R_0^2} \frac{\exp(2\eta_f)}{4} (\cos^2 \psi + \sin^2 \psi) = \frac{a^2}{R_0^2} \frac{\exp(2\eta_f)}{4}. \quad (25)$$

Then the right hand side of Eq. (19) becomes

$$\begin{aligned} & \frac{a^2}{R_0^2} \left\{ \frac{\exp(2\eta_f)}{4} \ln \left[\frac{a^2 \exp(2\eta_f)}{R_0^2 4} \right] - \frac{\exp(2\eta_f)}{4} \right\} = \\ & \frac{a^2}{R_0^2} \left\{ \frac{\exp(2\eta_f)}{4} \left[2\eta_f + \ln \left(\frac{a^2}{4R_0^2} \right) \right] - \frac{\exp(2\eta_f)}{4} \right\} \approx \frac{a^2}{R_0^2} \left[\frac{\eta_f \exp(2\eta_f)}{2} - \frac{\exp(2\eta_f)}{4} \right], \end{aligned} \quad (26)$$

since $2\eta_f \gg \ln(a^2 / 4R_0^2)$ and therefore can be neglected. Introducing the above expression in Eq. (19) makes it identical to (18). For very large η_f and one may use the approximation

$$x \ln x - x \approx \ln(x!) \approx \ln[\Gamma(x+1)], \quad (27)$$

which allows to write the left hand sides of Eq. (18) in a more compact form.

$$\frac{1}{8} \eta_f \exp(2\eta_f) - \frac{1}{16} \exp(2\eta_f) \approx \frac{1}{16} \ln[\Gamma(e^{2\eta_f} + 1)]. \quad (28)$$

IV. CAPILLARY DRIVEN FLOW IN EXPANDING THREE DIMENSIONAL POROUS MEDIA

A. Exact solution in 3D

For flow in 3D porous media, a general grasp of the geometry can be obtained from Figures 1a and 1b if the graphs are revolved around their vertical axis of symmetry (the z -axis in Figure 3). The coordinates that are relevant to such system are defined by²⁴ (see also Figure 3)

$$\begin{aligned}x &= a \cosh \eta \sin \theta \cos \psi \\y &= a \cosh \eta \sin \theta \sin \psi . \\z &= a \sinh \eta \cos \theta\end{aligned}\tag{29}$$

Note that the variable ψ is different from the one used in the elliptic 2D case discussed above (see Figure 3 and compare it to Figure 2). The Laplace equation for the flow potential, Eq. (4), has the form²⁴

$$\nabla^2 \varphi = \frac{1}{a^2 (\cosh^2 \eta - \sin^2 \theta)} \left(\frac{\partial^2 \varphi}{\partial \eta^2} + \tanh \eta \frac{\partial \varphi}{\partial \eta} + \frac{\partial^2 \varphi}{\partial \theta^2} + \cot \theta \frac{\partial \varphi}{\partial \theta} \right) + \frac{1}{a^2 \cosh^2 \eta \sin^2 \theta} \frac{\partial^2 \varphi}{\partial \psi^2} = 0.\tag{30}$$

Since we consider an axis-symmetric domain, $\partial^2 \varphi / \partial \psi^2 = 0$, the last term can be dropped. Additionally, there is no flow across the surface corresponding to $\theta = \pi/2$ and $\theta = -\pi/2$, hence there is no change with θ and all derivatives with respect to the polar angle are zero. Therefore Eq. (30) can be significantly simplified to

$$\frac{d^2 \varphi}{d\eta^2} + \tanh \eta \frac{d\varphi}{d\eta} = 0.\tag{31}$$

This equation describes concentric oblate surfaces that correspond to the flow potential $\varphi(\eta)$. The boundary conditions for capillary driven flow are identical to those given by Eq. (8)

$$\begin{aligned}\varphi &= \varphi_0 = -\frac{k}{\mu} P_C \text{ at } \eta = 0 \\ \varphi &= 0 \text{ at } \eta = \eta_f\end{aligned}\tag{32}$$

The solution for the flow potential is then

$$\varphi = \varphi_0 \left\{ 1 - \frac{\arctan [\tanh (\eta / 2)]}{\arctan [\tanh (\eta_f / 2)]} \right\}.\tag{33}$$

Note that for $\eta_f \rightarrow \infty$ the above expression becomes

$$\varphi = \varphi_0 \left\{ 1 - \frac{4 \arctan[\tanh(\eta/2)]}{\pi} \right\} \quad (34)$$

which means that in the 3D case we have a finite asymptotic result for infinite domains which is not true for the one and two dimensional cases.

The liquid velocity profile in the 3D porous region has only an η -component, which is

$$v_\eta = \frac{1}{a(\cosh^2 \eta - \sin^2 \theta)^{1/2}} \frac{\partial \varphi}{\partial \eta} = \frac{kP_C}{2\mu a \cosh \eta (\cosh^2 \eta - \sin^2 \theta)^{1/2} \arctan[\tanh(\eta_f/2)]}. \quad (35)$$

The velocity of the front is

$$v_{\eta_f} = \frac{1}{a(\cosh^2 \eta_f - \sin^2 \theta)^{1/2}} \left(\frac{\partial \varphi}{\partial \eta} \right)_{\eta=\eta_f} = \frac{kP_C}{2\mu a \cosh \eta_f (\cosh^2 \eta_f - \sin^2 \theta)^{1/2} \arctan[\tanh(\eta_f/2)]} \quad (36)$$

The velocity is formally expressed in terms of the spatial and temporal variables by

$$v_{\eta_f} = a(\cosh^2 \eta_f - \sin^2 \theta)^{1/2} \frac{d\eta_f}{dt}. \quad (37)$$

Hence, combining (36) and (37) one derives

$$\int_0^{\eta_f(t)} (\cosh^2 \eta_f' - \sin^2 \theta) \arctan \left[\tanh \left(\frac{\eta_f'}{2} \right) \right] \cosh \eta_f' d\eta_f' = -\frac{kP_C}{2\mu a^2} t = \frac{\tilde{t}}{2}. \quad (38)$$

After integration we obtain a relationship between the front position η_f and scaled time \tilde{t}

$$\begin{aligned} & \frac{1}{3} \arctan \left[\tanh \left(\frac{\eta_f}{2} \right) \right] \left[2 + 3 \cos(2\theta) + \cosh(2\eta_f) \right] \sinh(\eta_f) - \\ & \frac{1}{6} [1 + 3 \cos(2\theta)] \ln [\cosh(\eta_f)] - \frac{1}{12} [\cosh(2\eta_f) - 1] = \tilde{t} \end{aligned} \quad (39)$$

The front velocity is then obtained by introducing the obtained time dependence of η_f in Eq. (36) or (37). The volumetric flux is obtained from

$$\begin{aligned}
U(\tilde{t}) &= \int_A \mathbf{v} \cdot \mathbf{n} dA = \frac{kP_C}{\mu a} \frac{a^2}{\arctan \left\{ \tanh \left[\frac{\eta_f(t)}{2} \right] \right\}} \int_0^{2\pi} d\psi \int_0^{\theta_0} \sin \theta d\theta \\
&= \frac{2\pi a k P_C (1 - \cos \theta_0)}{\mu \arctan \left\{ \tanh \left[\frac{\eta_f(t)}{2} \right] \right\}}.
\end{aligned} \tag{40}$$

For full open entrance ($\theta_0 = \pi/2$)

$$U(\tilde{t}) = \frac{2\pi a k P_C}{\mu \arctan \left\{ \tanh \left[\frac{\eta_f(t)}{2} \right] \right\}}. \tag{41}$$

B. Asymptotic results for small and large η_f

For short times and small values of η_f and $\theta = 0$ Eq. (39) simplifies to

$$\frac{\eta_f^2}{2} = \tilde{t}. \tag{42}$$

The long-time, large η_f , asymptotic result can be derived for Eq. (42) using the same arguments as above [see Eq. (18)] and also noting that $\arctan \left[\tanh(\eta_f/2) \right] \rightarrow \pi/4$. The result is

$$\frac{\pi}{4} \frac{\exp(3\eta_f)}{12} = \tilde{t}. \tag{43}$$

For large η_f the front shape should approach that of an expanding sphere. The latter can be derived from Eq. (4) written in the form

$$\frac{1}{r^2} \frac{d}{dr} \left(r^2 \frac{d\varphi}{dr} \right) = 0 \tag{44}$$

together with the following boundary conditions

$$\begin{aligned}
r = R_0, \quad \varphi = \varphi_0 = -\frac{k}{\mu} \Delta P, \quad \Delta P = P_C \\
r = R_f, \quad \varphi = 0
\end{aligned}
\tag{45}$$

Then the solution for the potential is (see also Ref. ¹⁶)

$$\varphi = \varphi_0 \frac{R_f R_0}{R_f - R_0} \left(\frac{1}{r} - \frac{1}{R_f} \right).
\tag{46}$$

It is interesting to point out that in the case of 3D radial flow, there is a finite solution for $\varphi(r)$ even if R_f is at infinity. In this case

$$\varphi = \varphi_0 \frac{R_0}{r}.
\tag{47}$$

The radial velocity is then

$$v_r = \frac{\partial \varphi}{\partial r} = -\varphi_0 \frac{R_f R_0}{R_f - R_0} \frac{1}{r^2} = \frac{R_f R_0}{R_f - R_0} \frac{k P_C}{\mu} \frac{1}{r^2}.
\tag{48}$$

At $r = R_f$

$$v_{R_f} = \frac{dR_f}{dt} = \frac{R_0}{R_f (R_f - R_0)} \frac{k P_C}{\mu}.
\tag{49}$$

Hence the time-dependent position of the moving front is given by

$$\int_{R_0}^{R_f} \frac{R_f' (R_f' - R_0)}{R_0^3} dR_f' = \frac{R_f^3}{3R_0^3} - \frac{R_f^2}{2R_0^2} + \frac{1}{6} = \frac{a^2}{R_0^2} \tilde{t}.
\tag{50}$$

The radial coordinate in 3D oblate spheroid coordinates is

$$\begin{aligned}
r^2 = x^2 + y^2 + z^2 = \\
a^2 \left(\cosh^2 \eta \sin^2 \theta \cos^2 \psi + \cosh^2 \eta \sin^2 \theta \sin^2 \psi + \sinh^2 \eta \cos^2 \theta \right) = . \\
a^2 \left(\cosh^2 \eta \sin^2 \theta + \sinh^2 \eta \cos^2 \theta \right)
\end{aligned}
\tag{51}$$

At the front $\eta = \eta_f$ and for large η_f we use the approximations $\cosh^2 \eta \approx \exp(2\eta)/4$ and $\sinh^2 \eta \approx \exp(2\eta)/4$. Hence

$$\frac{R_f^2}{R_0^2} = \frac{a^2}{R_0^2} \frac{\exp(2\eta)}{4} \quad (52)$$

and Eq. (50) becomes

$$\begin{aligned} \frac{R_f^3}{3R_0^3} - \frac{R_f^2}{2R_0^2} + \frac{1}{6} &= \frac{a^3}{3R_0^3} \frac{\exp(3\eta)}{8} - \frac{a^2}{2R_0^2} \frac{\exp(2\eta)}{4} + \frac{1}{6} = \frac{a^2}{R_0^2} \tilde{t}, \quad \text{or} \\ \frac{a}{R_0} \frac{\exp(3\eta)}{24} - \frac{\exp(2\eta)}{8} + \frac{R_0^2}{6a^2} &= \tilde{t}. \end{aligned} \quad (53)$$

Keeping only the leading order term in (53) and expressing the ratio a/R_0 using Eq. (23) we obtain

$$\frac{\pi}{2} \frac{\exp(3\eta)}{24} = \tilde{t} \quad (54)$$

which is identical to (43).

V. RESULTS AND DISCUSSION

A. Transport in two dimensional porous media

Two effects govern the liquid transport in an expanding 2D porous region. Both of them follow from the mass conservation of the incompressible liquid. The first one follows from the mass conservation and is due to the liquid distribution over an ever-increasing space (or area). This effect leads to an apparent decrease in the velocity of the moving front. At the same time the liquid travels less distance per unit time which lowers the friction resistance while the capillary force increases due to the expansion of the front. The combination of the two effects slows down the linear velocity and facilitates the bulk flow rate in an expanding porous material. Figures 4a and 4b show the dependence of the liquid front position and linear velocity of capillary driven liquid flow in two dimensional porous regions. The solid lines correspond to the case depicted in Figure 1a (the entrance has finite dimensions). The plot was derived from Eq. (13) setting $\psi = \pi/2$ i.e., the flow along the y -axis is traced (see Figure 2). It is compared to the LW power-law case¹⁰⁻¹¹ of non-expanding porous material which maintains constant cross

sectional dimension [dashed line, see also Eqs. (16) and (17)], as well as to the case of radial flow¹⁷ [see Eq. (19)]. At short times the front position shows a power law increase similar to the LW solution. This is due to the fact that the effect of the expansion is weak for short distances, the liquid has not spread too much, and the streamlines are almost parallel. As time progresses, however, the expansion effect increases and the distance traveled by the front in the expanding porous domain decreases in comparison with the non-expanding LW case because liquid has also moved to the sides to form the elliptically shaped front. For long times the front becomes less elliptical and more circular and the solution for the front position asymptotically approaches that for an expanding circle given by the dotted line in Figure 4a [see Eqs. (18) and the discussion thereafter]. Hence, the LW¹⁰⁻¹¹ solution and the circular expansion result obtained by Hyväluoma et al.¹⁷ represent the limiting cases of no expansion and maximum expansion in 2D. Our result given by Eq. (13) describes the entire time behavior including two limiting cases as well as the intermediate case, and as seen from Figure 4a. The latter applies to a range of more than two orders of magnitude of the scaled time.

The time dependence of the linear velocity of the liquid front is shown in Figure 4b. The solid line corresponds to our solution given by Eq. (11) in combination with (13). The dashed line is the LW result¹⁰⁻¹¹ and the dotted line is that for the radial flow when R_f / R_0 or, equivalently, η_f are large.¹⁷ Clearly the velocity drops with time for all the cases but at different rates. If the porous region does not expand, then the reason for the velocity decrease is due to the increase of the length of liquid penetration. This length contributes to the viscous resistance and hence, slows down the motion. If the liquid travels in an expanding material (like the examples outlined in Figure 1) the front motion is also slowed by the fact that liquid is diverted sideways into the available expanding space. The effect of the expansion is strongest in the case of pure radial flow. At short times our solution is close to that for a non-expanding medium and asymptotically approaches the one for radial flow for very long times.

It is interesting to examine the dependence of the bulk (volumetric) flow rate since it is a measure of the ability of the porous material to absorb liquid. An important practical application exploiting this ability is to drive fluid in devices and material using capillary action instead of an external power source.⁴ The solid line in Figure 5 shows the change of the bulk flow rate with time calculated from Eq. (41). Since we are considering a 2D domain, the bulk flow rate is calculated per unit length in direction normal to the plane of the flow. Again for comparison both the non-expanding LW and the radial expanding cases (for large η_f) are shown. Both are obtained in a similar way by multiplying the liquid velocity at the front by its length. Clearly an expanding porous material has better capabilities of absorbing liquids; as it is evident in the plots, the bulk flow rate decreases much slower with time in comparison with the non-expanding case.

B. Transport in three dimensional porous media

The effect of expansion is stronger when it occurs in three dimensions. The reason is that there is more space available for the liquid to occupy as it moves forward driven by capillary

pressure. The calculations presented below are for fully opened medium where $\theta = \pi/2$ (see Figure 3). The entrance has a circular shape. The flow along the y -axis is traced, which corresponds to $\theta = 0$. Figure 6a shows the position of the fluid front as a function of the elapsed time. The solid line corresponds to the solution in oblate spheroid coordinates given by Eq. (39) (i.e. the fluid enters the porous material through a circular entrance with finite dimension) and it is compared to the non expanding case (dashed line) and the expansion in spherical symmetry for large R_f / R_0 [or η_f – see Eq. (54)]. At short times the expansion effect is insignificant while at long times the behavior approaches that of an expanding spherical front. Similarly to the 2D case, our solution interpolates between these two limiting cases and provides a correct description for the cases where the liquid enters the 3D expanding porous material through an entrance with a finite size.

The linear velocity of the advancing liquid front is shown in Figure 6b. The effect of the expansion on the front velocity resembles 2D (see Figure 4b) but more pronounced because of the spreading of the liquid over larger front area. That leads to greater reduction of the velocity of the moving liquid front.

The bulk volumetric velocity is presented in Figure 7. It should be emphasized that the 3D expanding case allows for a solution where fluid will keep entering the porous material through the circular entrance. This is also evident from Eq. (41) which for time and $\eta_f \rightarrow \infty$ becomes

$$\tilde{U}_\infty = \frac{\mu U_\infty}{2\pi a k P_c} = \frac{4}{\pi}. \quad (55)$$

This result implies that 3D porous media can be used as capillary pumps to drive fluids in devices. This cannot be accomplished if the porous material does not expand, or the expansion is two dimensional (see also the discussion below). The actual rate of drawing liquid in, however, will depend on parameters such as the average pore size, liquid viscosity, and pore wetting ability and may turn out in many cases to be too low (see experimental results in Xiao, et. al.¹⁶).

Since the asymptotic result (55) follows from the dimensionality of the system, one may expect that similar relationship to exist for the pure radial (spherical) transport (see Figure 7). Indeed using equation (48) we can find the linear velocity at the entrance where $r = R_0$. To obtain the bulk flow rate one needs to multiply the result by the area of the entrance which we assume to be a hemispherical in order to better compare to the oblate spheroid case discussed above. Thus the asymptotic ($R_f \rightarrow \infty$) expression reads

$$\tilde{U}_\infty = \frac{\mu U_\infty}{2\pi R_0 k P_c} = 1. \quad (56)$$

Hence, if the system is 3D stationary solutions are possible, which is generally the case for Laplace equations in infinite or semi-infinite spaces and is known for similar processes like heat transfer or diffusion.²⁵

C. Effect of porous media dimensionality

The dimensionality of the porous media is extremely important for the flow rate. There is no expansion in the case of 1D transport (which is represented by the LW case¹⁰⁻¹¹) and the linear velocity (as well as the bulk flow rate) drop as $1/\sqrt{t}$. At the other extreme, the 3D case allows for a solution even for $\eta_f \rightarrow \infty$ [see Eq. (55) above]. Figure 8a shows a comparison for the time dependent position of the moving liquid front for 1D, 2D (elliptical) and 3D (oblate spheroid) cases. The 1D case exhibits the farthest liquid penetration while in 2D and 3D the distance is much shorter. The rate of liquid motion also decreases with the dimensionality of the flow (see Figure 8b). This is due to distribution of the advancing liquid over greater space. The cross sectional area that the fluid moves through does not change in 1D, increases linearly with distance in 2D, and quadratically in 3D. Since the liquid is incompressible it can cover shorter distances per unit time for the two and particularly the three dimensional cases. It is, however, very different for the bulk flow rate (see Figure 8c). The volume absorbed per unit time by the porous domain decreases the fastest for the 1D flow. The decrease in the bulk flow rate for 2D expanding case is lower and for 3D it levels off to a steady state [see Eq. (55) above]. The reason is the bulk flow rate is slowed down by the viscous resistance which increases with the length of the traveled path. The latter is greatest in 1D, shorter in 2D and shortest in 3D.

VI. CONCLUSIONS

We derived solutions for potential capillary driven liquid flow in 2D and 3D expanding porous media. The selection of suitable coordinate systems allows for simplification of the mass balance expressions to ordinary differential equations that can be exactly solved. The obtained solutions for expanding 2D and 3D porous materials are different from the well-known Lucas-Washburn solution describing liquid motion in non-expanding material geometries. The functional forms of the time dependence of the front position and velocity are more complicated if the porous domain is expanding. At the same time and the liquid linear velocity is lower, which is due to spreading of the incompressible liquid over an ever-increasing domain.

The bulk flows display a qualitative difference in 1D, 2D and 3D. It decreases the fastest if the porous domain does not expand, less in 2D expanding domain and least in 3D. In fact the 3D case can reach a steady state for the bulk flow into the porous material. This makes it suitable to use in driving fluids through devices using capillary forces and without the need of an external power source.

ACKNOWLEDGEMENTS

This work was funded by NSF CAREER (CBET 0844645) and DoE-EPSCoR Implementation Program (DE-FG02-08ER46530).

References

1. T.D. Wheeler and A.D. Stroock, *The transpiration of water at negative pressures in a synthetic tree*. *Nature*, 2008. **455**: p. 208-212.
2. E.M. Fenton, M.R. Mascarenas, G.P. López, and S.S. Sibbett, *Multiplex Lateral-Flow Test Strips Fabricated by Two-Dimensional Shaping*. *ACS Appl. Mater. Interfaces*, 2009. **1**: p. 124–129.
3. A.W. Martinez, S.T. Phillips, and G.M. Whitesides, *Diagnostics for the Developing World: Microfluidic Paper-Based Analytical Devices*. *Anal. Chem.*, 2010. **82**: p. 3–10.
4. S. Mendez, E.M. Fenton, G.R. Gallegos, D.N. Petsev, S. Sibbett, H.A. Stone, Y. Zhang, and G.P. Lopez, *Imbibition in Porous Membranes of Complex Shape: Quasi-stationary Flow in Thin Rectangular Segments*. *Langmuir*, 2010. **26**: p. 1380–1385.
5. N.V. Churaev, *Liquid and Vapour Flows in Porous Bodies: Surface Phenomena*. *Topics in Chemical Engineering*, ed. A. Callwey. Vol. 13. 2000, New York: Gordon and Breach.
6. F.A.L. Dullien, *Porous Media: Fluid Transport and Pore Structure*. 1979, New York: Academic Press.
7. S.S.D. Julio and W.H. Shallenberger, *Bioslurping – Horizontal Radial Flow –Theory and Experimental Validation*. *J. Hazardous Substance Res.*, 2002. **3**: p. 6-1 -- 6-19.
8. J. Ge, R. Schirhagl, and R.N. Zare, *Glucose-Driven Fuel Cell Constructed from Enzymes and Filter Paper*. *J. Chem. Educ.*, 2011. **88**: p. 1283–1286.
9. J.M. Bell and F.K. Cameron, *The flow of liquids through capillary spaces*. *J. Phys. Chem.*, 1906. **10**: p. 658–674.
10. R. Lucas, *Ueber das Zeitgesetz des Kapillaren Aufstiegs von Flüssigkeiten*. *Kolloid Z.*, 1918. **23**: p. 15.
11. E.W. Washburn, *The Dynamics of Capillary Flow*. *Phys. Rev.*, 1921. **17**: p. 273-283.
12. J. Happel and H. Brenner, *Low Reynolds Number Hydrodynamics*. *Mechanics of fluids and transport processes*, ed. R.J. Moreau. 1983, Boston: Kluwer.
13. C. Hall, *Water Movement in Porous Building Materials--IV. The Initial Surface Absorption and the Sorptivity*. *Build. Environ.*, 1981. **16**: p. 201-207.
14. M.A. Wilson, W.D. Hoff, and C. Hall, *Water.Movement in Porous Building Materlals XI. Capillary Absorption from a Hemispherical Cavity*. *Build. Environ.*, 1994. **29**: p. 99-104,.
15. J.R. Philip. *Absorption and infiltration in two- and threedimensional systems*. in *UNESCO Symposium on Water in the Unsaturated Zone; International Association for Scientific Hydrology*. 1996. Wageningen.
16. J. Xiao, H.A. Stone, and D. Attinger, *Source-like Solution for Radial Imbibition into a Homogeneous Semiinfinite Porous Medium*. *Langmuir*, 2012. **28**: p. 4208–4212.
17. J. Hyväluoma, P. Raiskinmäki, A. Jäsberg, A. Koponen, M. Kataja, and J. Timonen, *Simulation of liquid penetration in paper*. *Phys. Rev. E*, 2006. **73**: p. 036705.
18. J.R. Philip, *Theory of Infiltration*, in *Advances in Hydrosience*, W. Chou, Editor. 1969, Academic Press: New York. p. 215-296.
19. R.J. Gummerson, C. Hall, W.D. Heft, R. Hawkes, G.N. Holland, and W. S. Moore, *Unsaturated water flow within porous materials observed by NMR imaging*. *Nature*, 1979. **281**: p. 56-57.
20. B. Lavi, A. Marmur, and J. Bachmann, *Porous Media Characterization by the Two-Liquid Method: Effect of Dynamic Contact Angle and Inertia*. *Langmuir*, 2008. **24**: p. 1918-1923.
21. E. Benner and D.N. Petsev, *in preparation*.
22. J.O. Wilkes, *Fluid Mechanics for Chemical Engineers with Microfluidics and CFD*. 2006, New York: Prentice Hall.
23. J.S. Rowlinson and B. Widom, *Molecular Theory of Capillarity*. 1982, Oxford: Clarendon Press.
24. P.H. Moon and D.E. Spencer, *Field Theory Handbook: Including Coordinate Systems, Differential Equations and Their Solutions*. 1988, New York: Springer.

25. L.D. Landau and E.M. Lifshitz, *Fluid Mechanics*. 1987, Amsterdam: Elsevier.

Figures

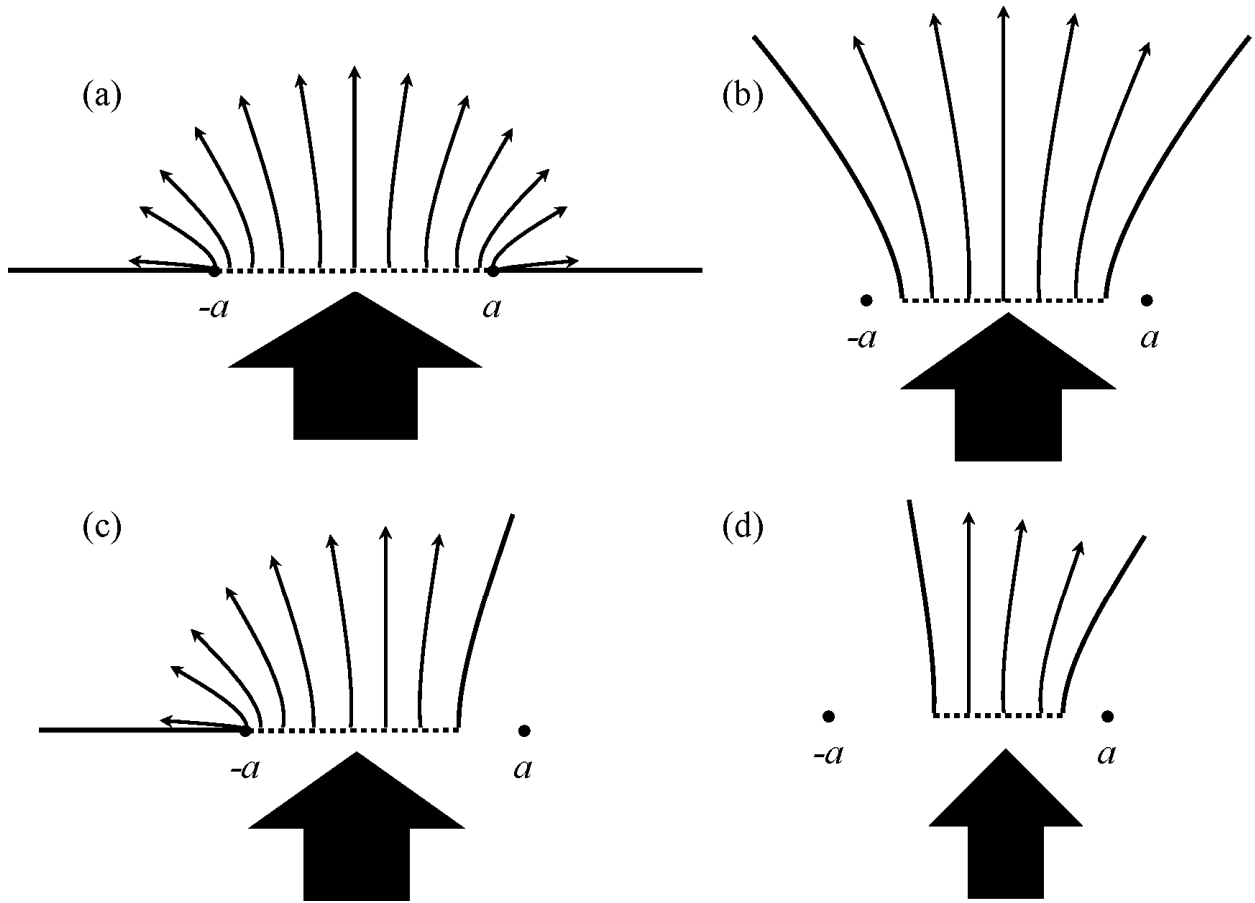


Figure 1. Examples for flows in various types of expanding porous media in 2D [see Eqs. (5) and Figure 2.] Case (a) corresponds to $0 \leq \psi \leq \pi$. Case (b) corresponds to $\psi_1 \leq \psi \leq \pi - \psi_1$ where ψ_1 is an arbitrary angle. Case (c) corresponds to $\psi_1 \leq \psi \leq \pi$. Case (d) corresponds to $\psi_1 \leq \psi \leq \pi/2$. Rotating cases (a) and (b) around the y-axis gives a 3D flow in expanding media [see Eqs. (29) and Figure 3] with $0 \leq \theta \leq \pi/2$ and $0 \leq \theta \leq \theta_1$ respectively, where θ_1 is an arbitrary angle.

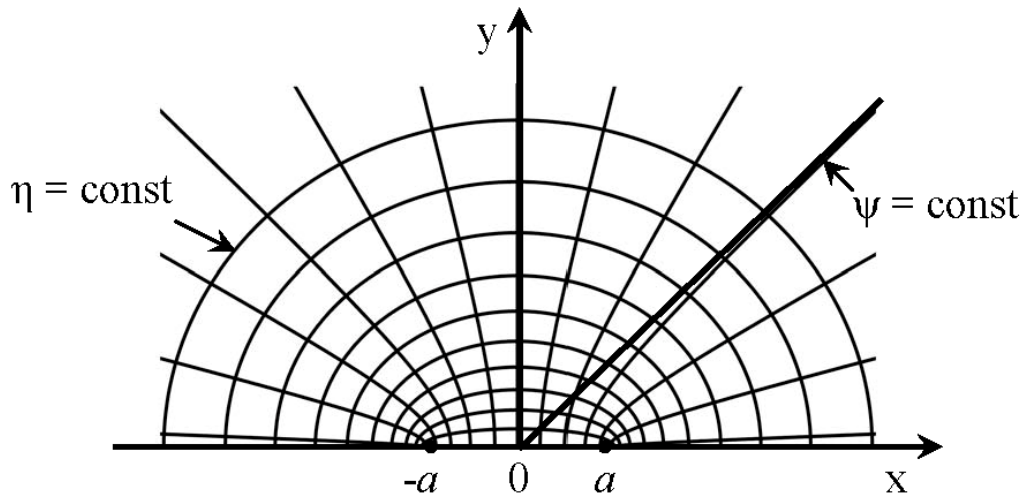


Figure 2. Elliptic coordinates, used to describe the flow in an expanding 2D porous domain. The points $-a$ and a are the foci of the ellipses.

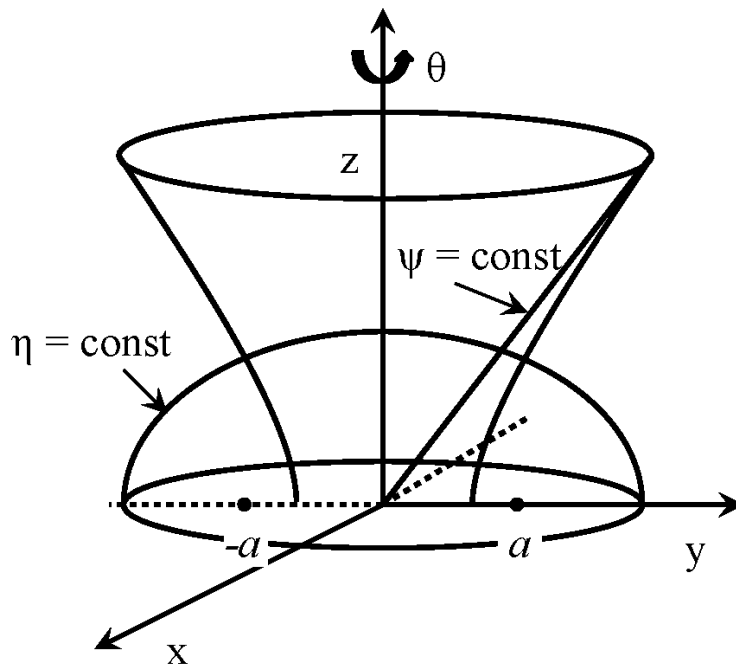


Figure 3. Oblate spheroid coordinates, used to describe the flow in an expanding 3D porous domain. The points $-a$ and a are the foci of the oblate surface corresponding to η . Only systems with axial symmetry are considered.

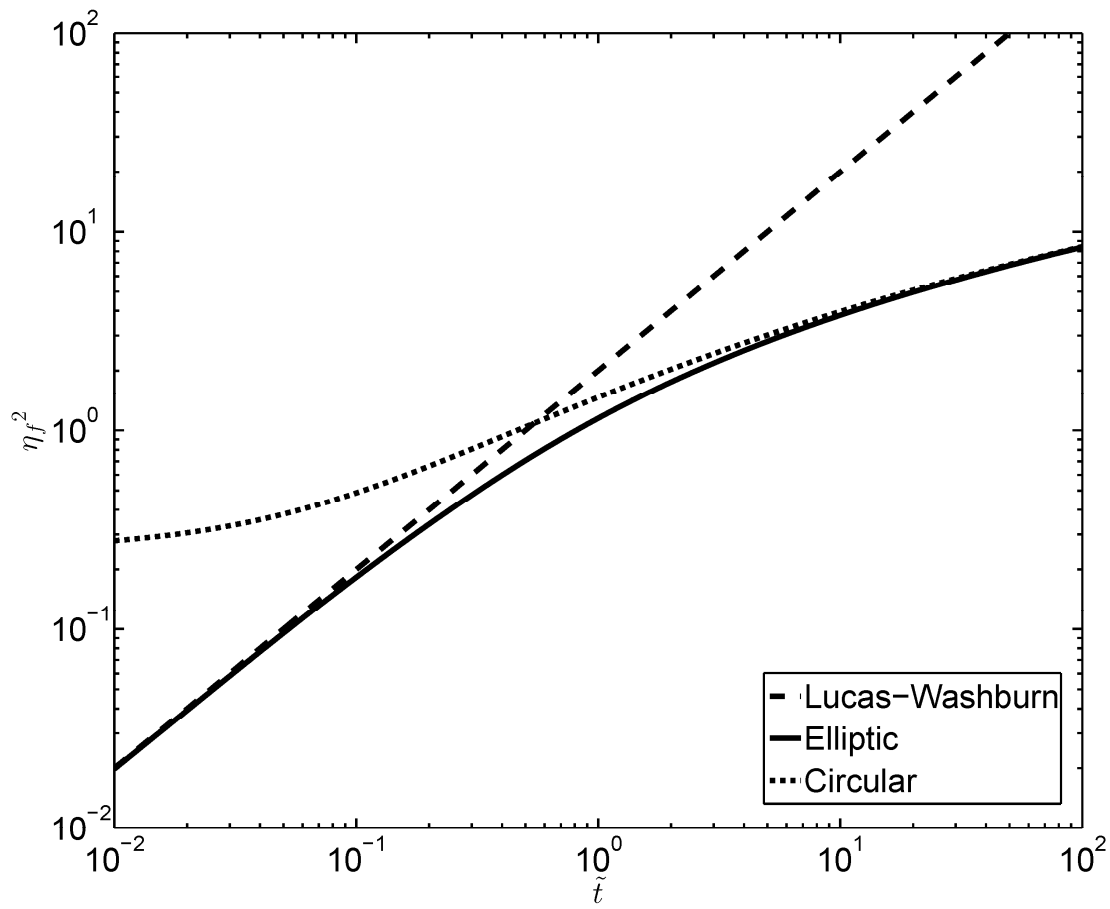


Figure 4a. Position of the liquid front in an expanding 2D porous material as a function of time [see Eq. (13)] (solid line). The dashed line is corresponds to the non-expanding LW result [see Eq. (16)]. The dotted line represents the result for an expanding circular front [see Eq. (19)].

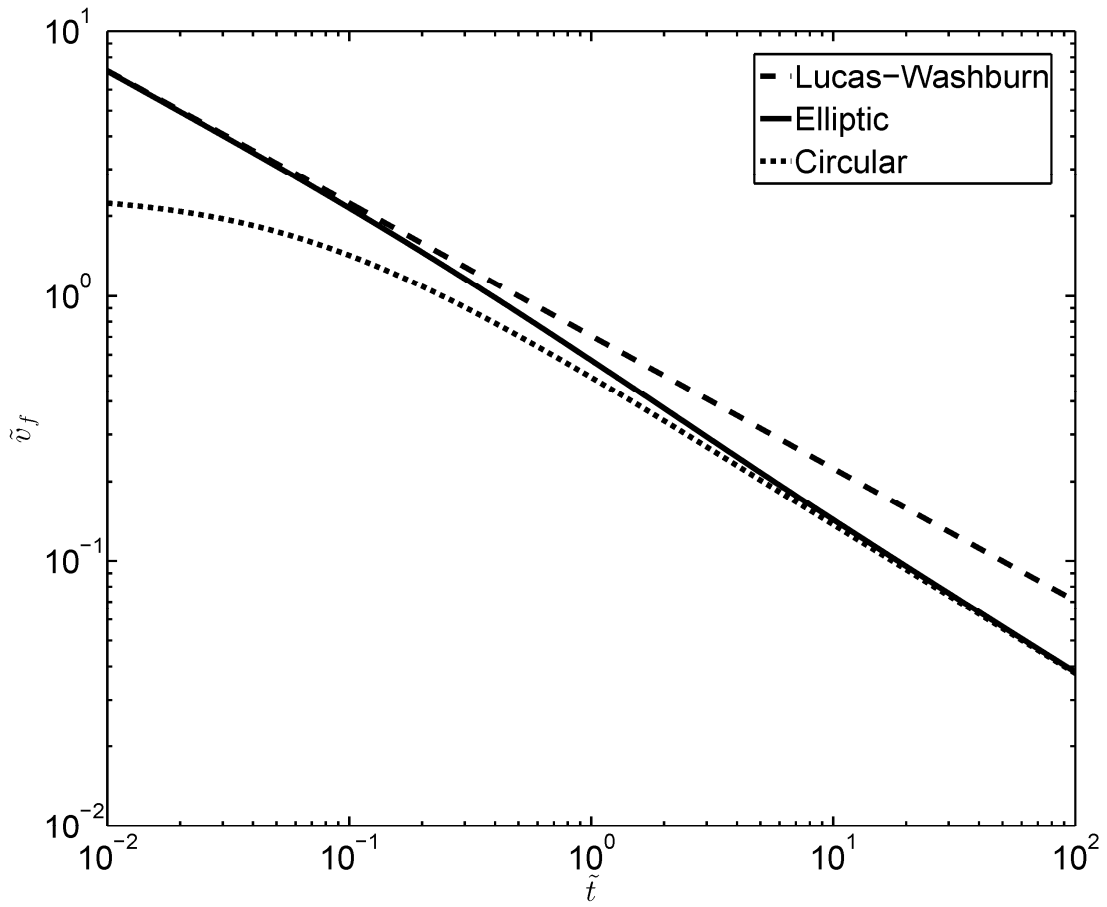


Figure 4b. Velocity of the liquid front for capillary motion in expanding 2D porous material. The solid line corresponds to the flow depicted in Figure 1a [see also Eqs. (11) and (13)]. The dashed line shows the LW while the dotted – the 2D radial flows.

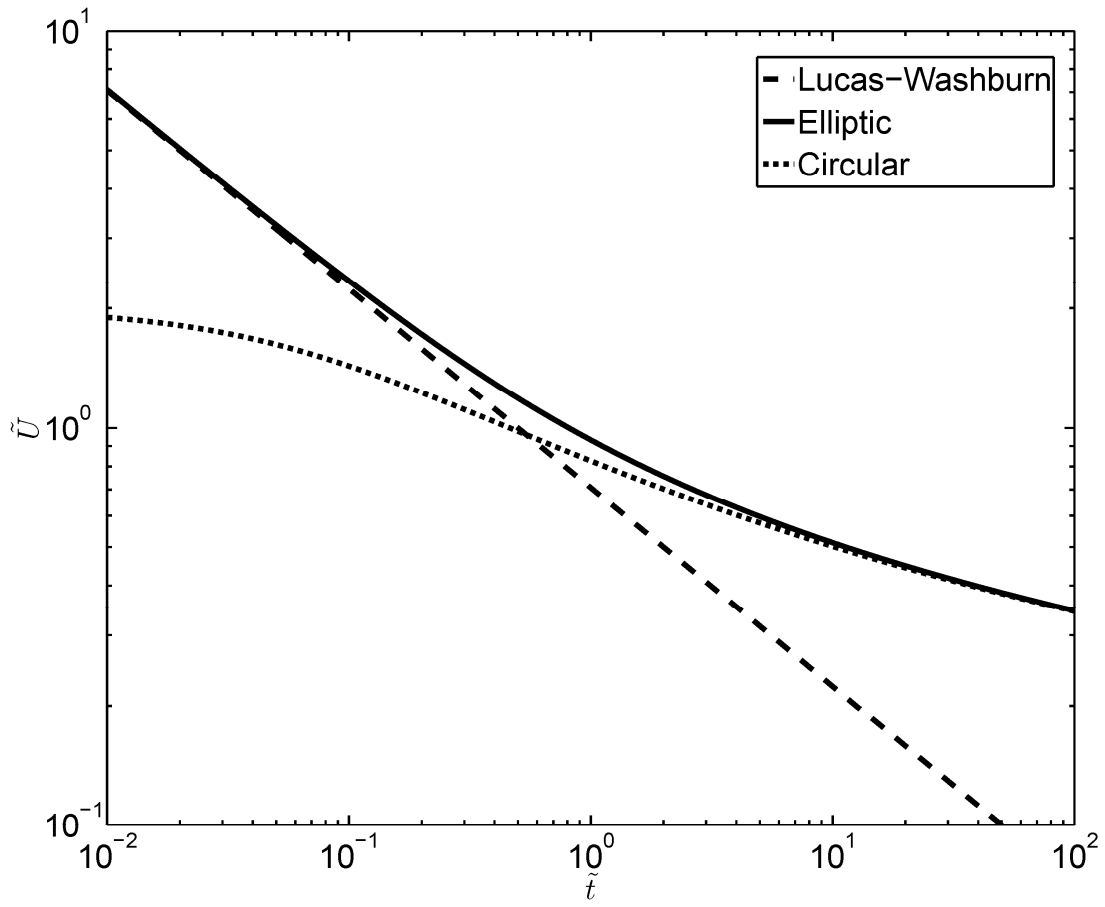


Figure 5. Bulk flow rate vs. time for expanding 2D porous materials. The solid line corresponds to the flow depicted in Figure 1a [see Eq. (15) and (13)]. The dashed line shows the LW while the dotted – the 2D radial flows for large η_f .

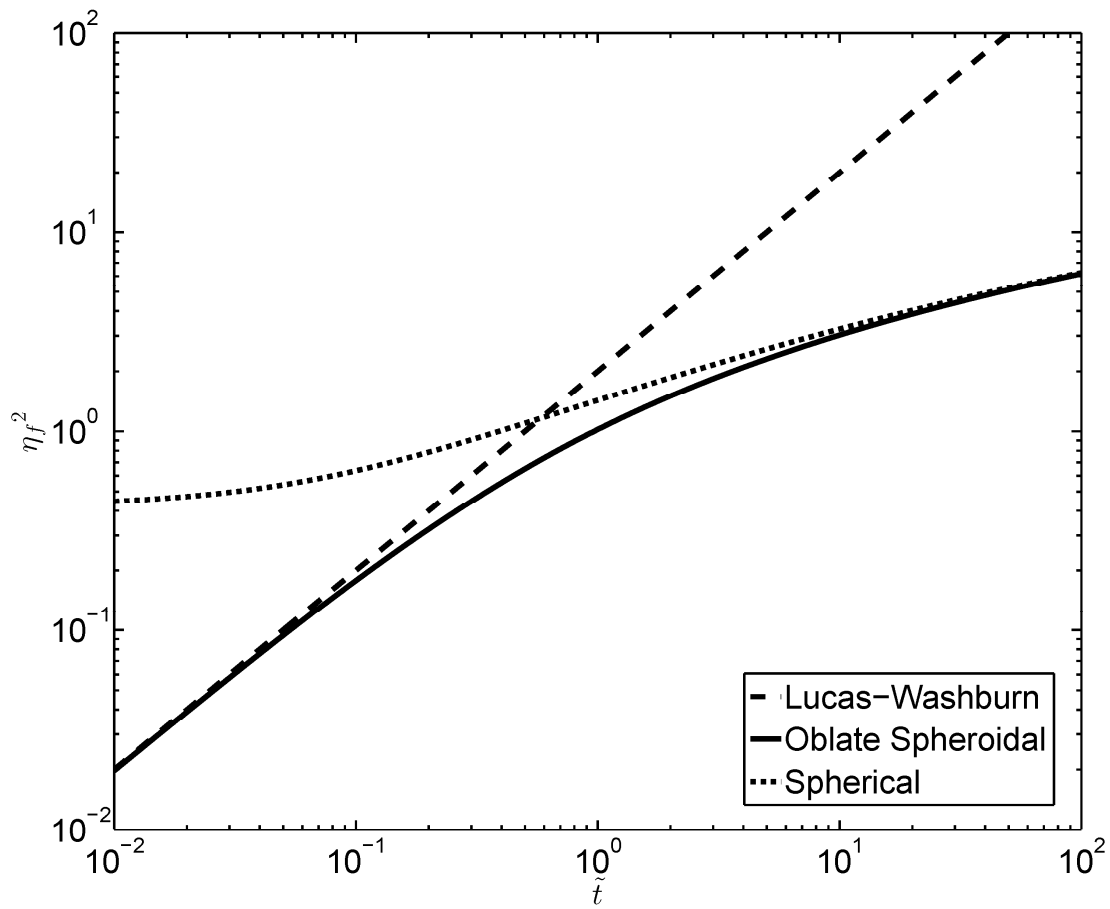


Figure 6a. Liquid front position as a function of the elapsed time in a 3D expanding porous material. The solid line corresponds to the solution in oblate spheroid coordinates, the dashed line is the LW non-expanding case and the dotted line is the solution for spherical expansion at large η_f .

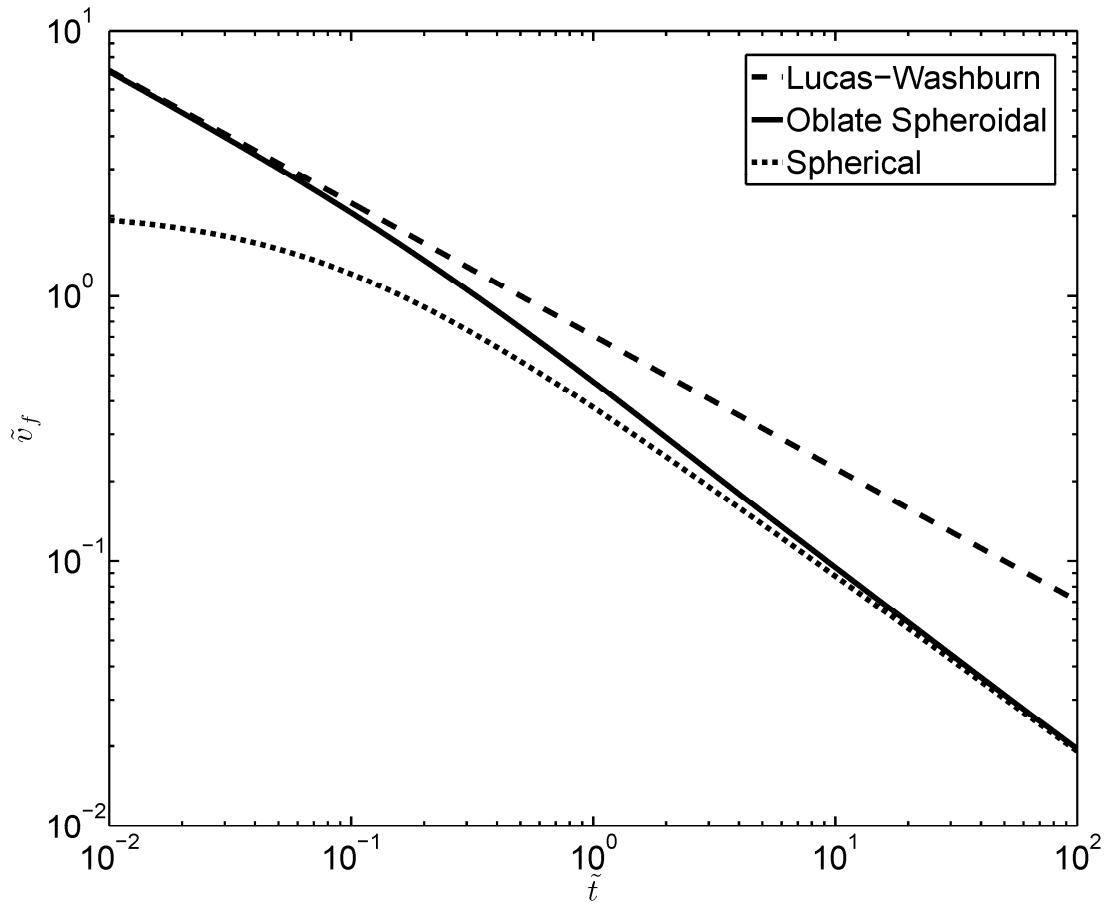


Figure. 6b. Linear velocity of the moving liquid front in 3D porous material. The solid line represents the solution for an oblate spheroid front, the dashed line is for the LW solution and the dotted line corresponds to the asymptotic case of an expanding spherical front.

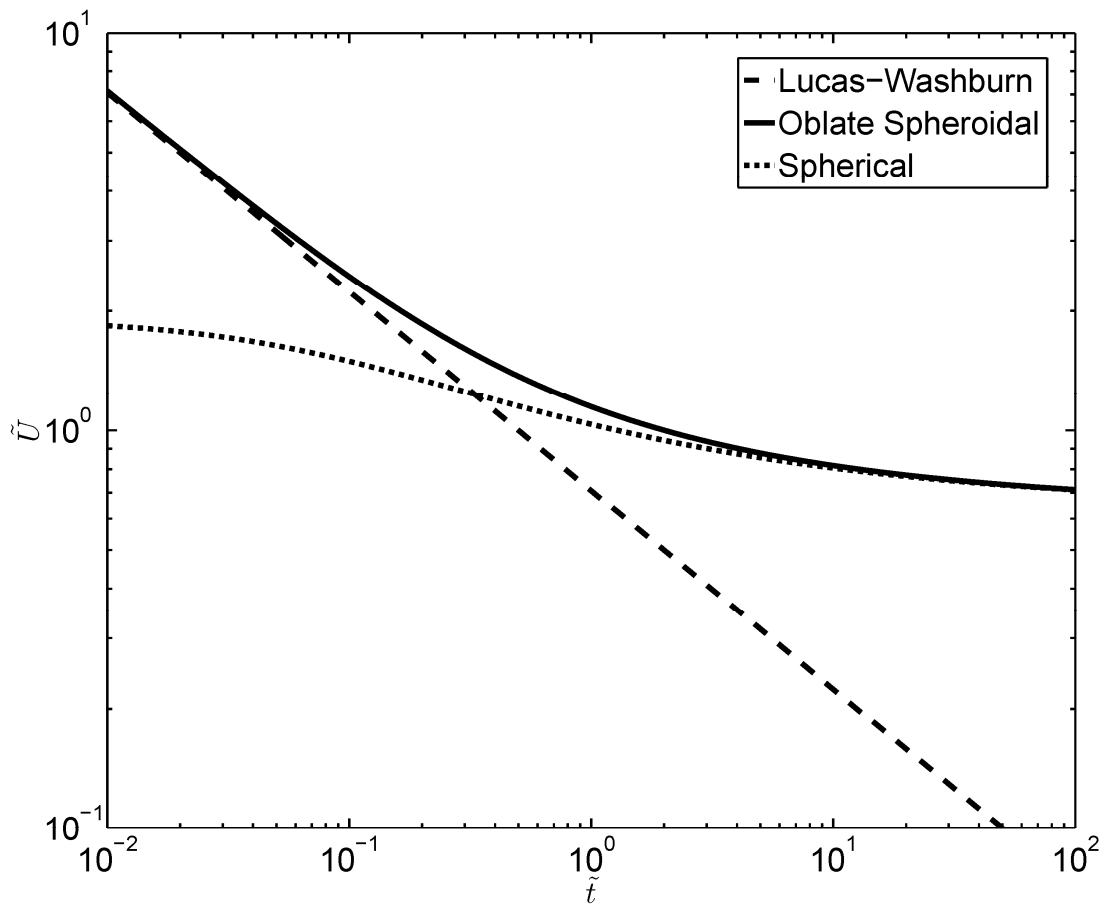


Figure 7. Bulk flow in 3D porous medium. The solid line the result for oblate spheroid symmetry, the dashed line corresponds to the LW case and dotted line represents the spherical case.

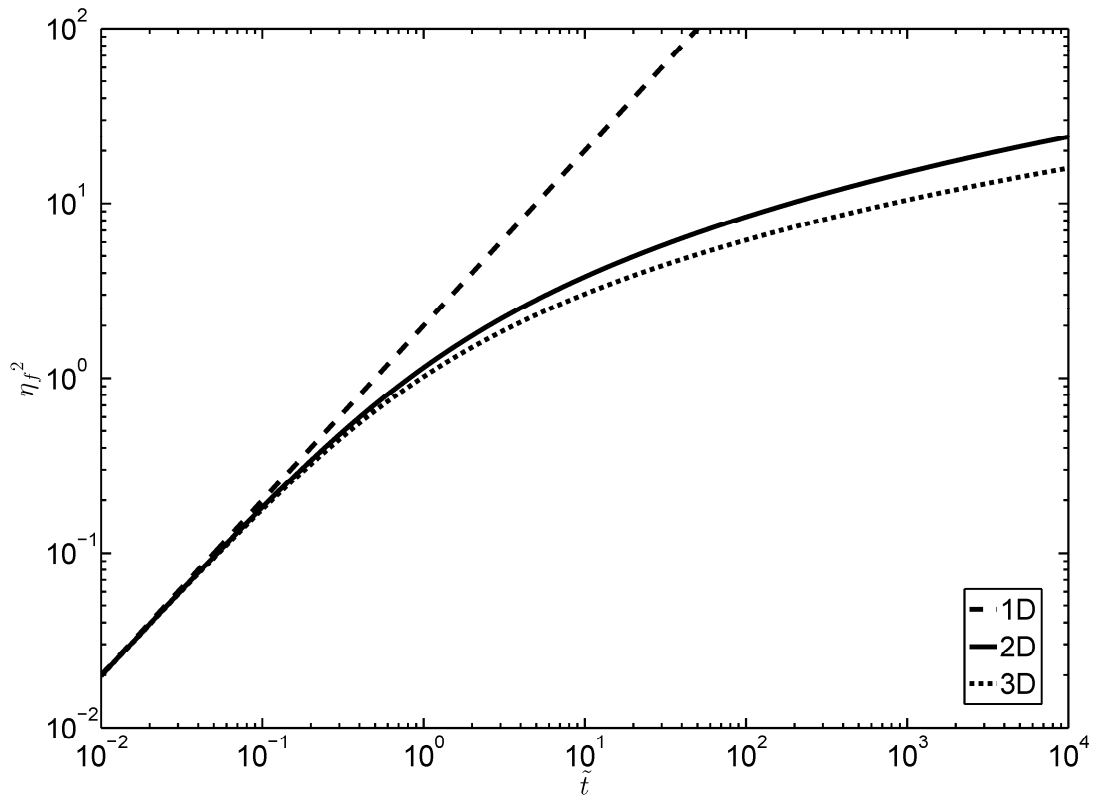


Figure 8a. Liquid front position vs. time in 1D (dashed line), 2D (solid line), and 3D (dotted line).

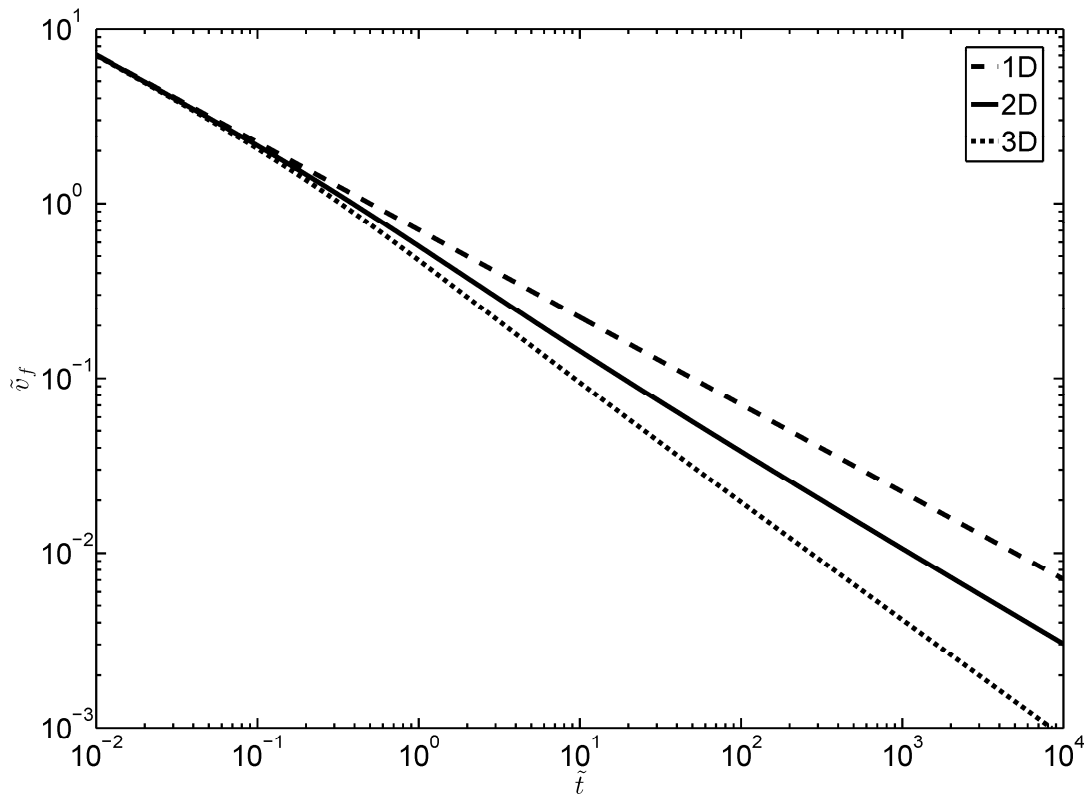


Figure 8b. Linear velocity of the liquid front vs. time in 1D (dashed line), 2D (solid line), and 3D (dotted line).

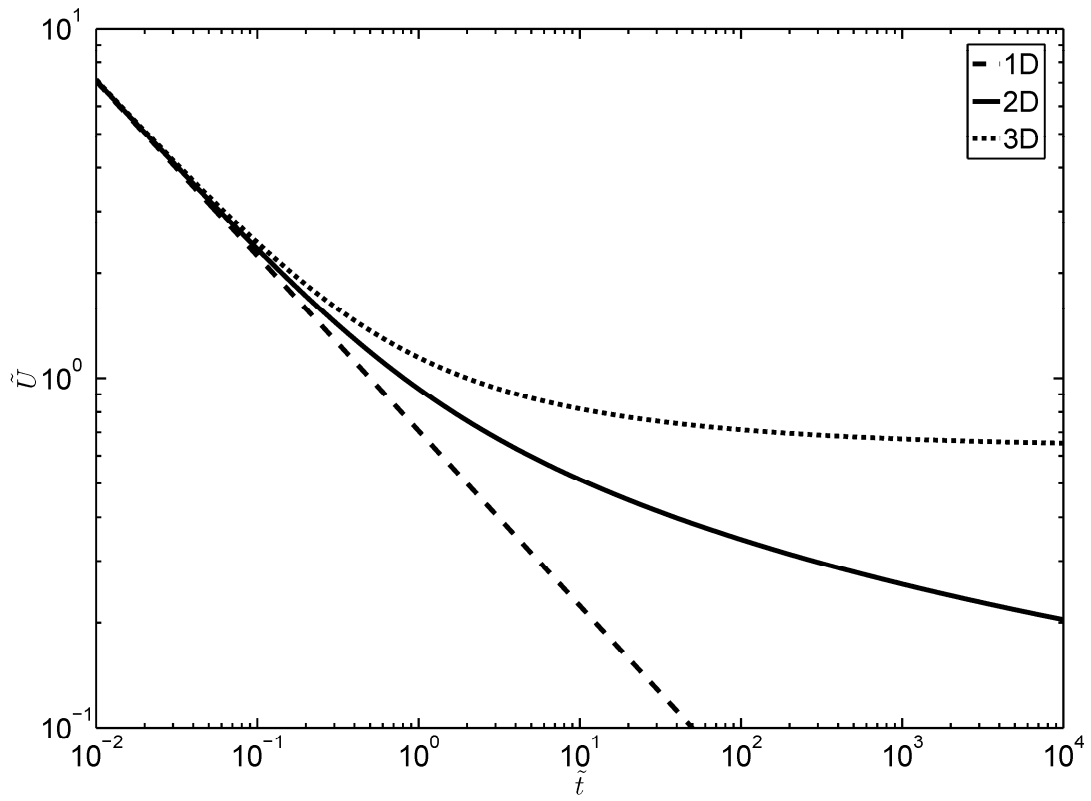


Figure 9. Bulk liquid flow vs. time in 1D (dashed line), 2D (solid line), and 3D (dotted line).